

Argonne National Laboratory

**ANALYSIS OF THE LINEAR COMPONENTS OF THE
POWER-REACTIVITY DECREMENT (PRD)
IN EBR-II**

by

John T. Madell and Richard E. Jarka

The facilities of Argonne National Laboratory are owned by the United States Government. Under the terms of a contract (W-31-109-Eng-38) between the U. S. Atomic Energy Commission, Argonne Universities Association and The University of Chicago, the University employs the staff and operates the Laboratory in accordance with policies and programs formulated, approved and reviewed by the Association.

MEMBERS OF ARGONNE UNIVERSITIES ASSOCIATION

The University of Arizona	Kansas State University	The Ohio State University
Carnegie-Mellon University	The University of Kansas	Ohio University
Case Western Reserve University	Loyola University	The Pennsylvania State University
The University of Chicago	Marquette University	Purdue University
University of Cincinnati	Michigan State University	Saint Louis University
Illinois Institute of Technology	The University of Michigan	Southern Illinois University
University of Illinois	University of Minnesota	University of Texas
Indiana University	University of Missouri	Washington University
Iowa State University	Northwestern University	Wayne State University
The University of Iowa	University of Notre Dame	The University of Wisconsin

LEGAL NOTICE

This report was prepared as an account of Government sponsored work. Neither the United States, nor the Commission, nor any person acting on behalf of the Commission:

A. Makes any warranty or representation, expressed or implied, with respect to the accuracy, completeness, or usefulness of the information contained in this report, or that the use of any information, apparatus, method, or process disclosed in this report may not infringe privately owned rights; or

B. Assumes any liabilities with respect to the use of, or for damages resulting from the use of any information, apparatus, method, or process disclosed in this report.

As used in the above, "person acting on behalf of the Commission" includes any employee or contractor of the Commission, or employee of such contractor, to the extent that such employee or contractor of the Commission, or employee of such contractor prepares, disseminates, or provides access to, any information pursuant to his employment or contract with the Commission, or his employment with such contractor.

Printed in the United States of America
Available from

Clearinghouse for Federal Scientific and Technical Information
National Bureau of Standards, U. S. Department of Commerce
Springfield, Virginia 22151

Price: Printed Copy \$3.00; Microfiche \$0.65

ARGONNE NATIONAL LABORATORY
9700 South Cass Avenue
Argonne, Illinois 60439

ANALYSIS OF THE LINEAR COMPONENTS OF THE
POWER-REACTIVITY DECREMENT (PRD)
IN EBR-II

by

John T. Madell* and Richard E. Jarka

EBR-II Project

October 1969

*Now with the Reactor Physics Division.

TABLE OF CONTENTS

	<u>Page</u>
ABSTRACT	7
I. INTRODUCTION.	7
II. DESCRIPTION OF THE NEUTRONIC MODEL	9
III. PHYSICAL MODEL FOR COMPONENTS OF THE PRD	10
A. Sodium in the Core (Case A)	10
B. Sodium in the Upper Reflector (Case B).	11
C. Sodium in the Inner-reflector/Blanket Region (Case C) . . .	11
D. Sodium throughout the Reactor (Case D)	11
E. Fuel Expansion (Case E).	12
F. Axial Expansion of Steel (Case F).	12
G. Combined Radial and Axial Expansion of Steel (Case G) . . .	13
H. 45-MWt Operation with No Radial Expansion (Case H)	14
I. 45-MWt Operation with Radial and Axial Expansion (Case I). .	14
IV. PREPARATION OF INPUT DATA FOR NEUTRONIC CODES . .	14
V. RESULTS AND DISCUSSION	18
A. Major Features of Runs 16, 24, 25, 26, 27, and 27'	18
B. Presentation of Results	19
C. Discussion of the Components of the PRD	19
1. Sodium in the Core	20
2. Sodium in the Upper Reflector.	20
3. Sodium in the Inner Reflector	20
4. Sodium in the Reactor	21
5. Fuel Expansion.	21
6. Axial Expansion of Steel.	21
7. Combined Radial and Axial Expansion of Steel	21

TABLE OF CONTENTS

	<u>Page</u>
D. Discussion of the Temperature and Expansion Coefficients	22
1. Sodium in the Core	22
2. Temperature Coefficient of Sodium in the Upper Reflector.	23
3. Temperature Coefficient of the Fuel.	23
4. Sodium in the Inner Reflector	23
5. Expansion Coefficients of Fuel and Steel.	23
E. Internal Consistency of the Calculated Values.	24
VI. FURTHER INVESTIGATION OF RADIAL MOTION	25
VII. OTHER RELATED REACTIVITY EFFECTS	27
A. Loss of Fuel-expansion Coefficient in Some Fuel Subassemblies	27
B. Reactivity Changes due to Slumping of Fuel Pins.	29
VIII. COMPARISON OF CALCULATED AND MEASURED VALUES.	30
REFERENCES	32

LIST OF FIGURES

<u>No.</u>	<u>Title</u>	<u>Page</u>
1.	Total, Linear, and Nonlinear Components of the PRD between 0 and 45 MWt for EBR-II Run 24	8
2.	Regional Representation of EBR-II for Two-dimensional (r, z) Calculations.	10
3.	Structure of ASPIRN Input Deck.	16
4.	PRD Curve for Run 24 Presented as Three Linear Segments . .	26

LIST OF TABLES

<u>No.</u>	<u>Title</u>	<u>Page</u>
I.	Temperatures by Material and Region in Runs 16, 24, 25, 26, 27, and 27' of EBR-II	10
II.	Radial and Axial Dimensional Boundaries for the Regional Representation of EBR-II.	15
III.	Quantities Used in Correcting Material Density for Expansion in the PRD Components.	16
IV.	Punched-card Specifications for Changing the Density of Material and/or Composition in ASPIRN Code	17
V.	Outline of Calculations Performed on Base Case to Obtain Components of the PRD	17
VI.	Description of EBR-II Core Loadings for Runs 16, 24, 25, 26, 27, and 27'	18
VII.	Values of PRD Components for Runs 16, 24, 25, 26, 27, and 27'.	19
VIII.	Temperature and Expansion Coefficients for Runs 16, 24, 25, 26, 27, and 27'	19
IX.	Average Material Temperatures and Expansions for Runs 16, 24, 25, 26, 27, and 27'	22
X.	Isothermal Expansion and Compaction Coefficients of the Core, Blanket, and Reflector for Runs 16, 24, 25, and 26	25
XI.	Predicted Pattern of Radial Motion of Subassemblies during an Approach to Power	27
XII.	EBR-II Loading for the Study of the Influence of Oxide-fueled Experimental Subassemblies on the Fuel-expansion Coefficient	28
XIII.	Results of Study of Fuel Expansion with Mixed-oxide Subassemblies	28
XIV.	Compositions, Dimensions, and Eigenvalues of an EBR-II Run-25 Subassembly with and without Fuel Slumping	29

ANALYSIS OF THE LINEAR COMPONENTS OF THE POWER-REACTIVITY DECREMENT (PRD) IN EBR-II

by

John T. Madell and Richard E. Jarka

ABSTRACT

This report defines the linear components of the power-reactivity decrement (PRD) and describes their representation for the neutronic calculations. The computer processing of the input specifications for the PRD calculations of six loadings of EBR-II is explained, and the results of the calculations are presented.

The results indicate that the linear components of the PRD are of the same magnitude for the six loadings. However, small trends in some linear components are observed with changes in core size and substitution of materials in the inner-blanket region.

The analytical results compare favorably with the results of the limited amount of experimental data available. The experimental data and recent analytical work suggest that a higher value of the linear-expansion coefficient of the fuel should be used in the PRD calculations.

Results of an investigation of two related reactivity effects--partial loss of fuel-expansion coefficient and slumping of fuel--are presented.

I. INTRODUCTION

This report describes an investigation of the linear components of the power-reactivity decrement (PRD) and provides detailed information to supplement the overall report¹ on the change in the PRD of EBR-II.

As the reactor power increases, the reactivity of the system changes. These changes are caused by changes in the physical properties of the system; this report considers those changes related only to temperature variations. The reactivity change from nonlinear effects is a function

of the temperature gradient as well as of the temperature. Changes in reactivity with power vitally affect the control and safety of the reactor. The reactor designer usually prefers a negative and prompt change of reactivity with increasing power.

In this report, the PRD is first divided into linear components, and the values of these components are calculated for various loadings of EBR-II between 0 and 45-MWt power. The magnitudes of both the PRD and the physical changes are very small for these loadings. All methods used to calculate changes in the system and in the reactivity therefore must be accurate, consistent, and reliable. Because of the importance of accurately describing the small changes, the method of calculating them is discussed in some detail. This report is concerned only with static analysis; dynamic considerations of reactivity change are not considered. The reactor is assumed to be at equilibrium for each calculation, and the total PRD for EBR-II is

measured at the beginning and end of each run. However, since all the individual components of a system such as EBR-II cannot be measured, the comparisons between experimental values and calculations are somewhat limited. In some instances, the exact physical situation cannot be represented in the calculational model; these instances will be noted when the results are discussed.

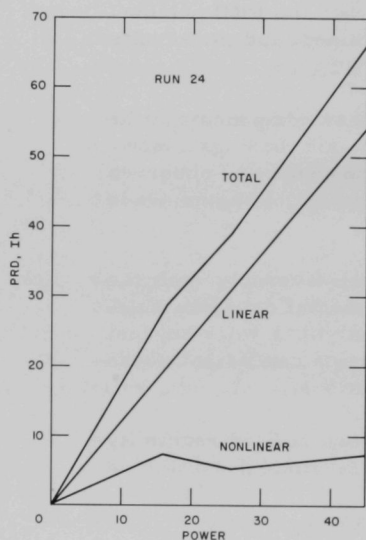


Fig. 1. Total, Linear, and Nonlinear Components of the PRD between 0 and 45 MWt for EBR-II Run 24

The interpretation of the PRD curves for Run 24 (Fig. 1) explains the role of the linear and nonlinear components. As the power increases from 0 to 45 MWt, the linear components appear as a straight line. The decrement is due to axial expansion of the fuel and steel and to changes in density of the reactor materials. The linear and volumetric expansion coefficients are assumed to be constant over the range of temperatures observed in EBR-II between 0 and 45 MWt. Moreover, reactivity changes are assumed to be linear with changes in density and dimensions over the range of densities and dimensions of interest.

Since the material temperatures at a given position vary linearly with power, the density changes and axial expansion are considered to be linear components of the PRD.

The predicted curve representing the nonlinear component has a positive slope initially; the slope of the curve becomes negative at about

16.5 MWt and becomes positive again at 25.5 MWt. The initial positive decrement of the nonlinear component is due to an outward bowing of the fuel and blanket subassemblies. At 16.5 MWt, in this case, the subassemblies are restrained from further outward movement at the top, and the middle subassemblies move inward to contribute a negative component to the PRD. After the middle subassemblies become compacted (at 25.5 MWt for Run 24), outward radial expansion produces a positive component of the PRD again. The nonlinear component has been analyzed in greater detail in several reports.^{2,3}

II. DESCRIPTION OF THE NEUTRONIC MODEL

Several factors were considered in selecting the neutronic model for calculating the linear components of the PRD. As was mentioned in Section I, the magnitude of changes in the physical system and in the reactivity is very small. The total PRD is of the order of 0.2% $\Delta k/k$; density and dimensional changes are normally less than 0.1% for a power increase from 0 to 45 MWt. The input data must accurately reflect the small physical changes to five significant figures; thus the eigenvalue convergence criteria must be about 1×10^{-6} .

EBR-II is at least two-dimensional in its neutronic characteristics;⁴ therefore, the changes in the reactivity must be described in a two-dimensional representation of the system. For example, neutron leakage in both the axial and radial directions contributes significantly to the reactivity change. Since the radial and axial leakages are not separable, they must be treated as one in a two-dimensional model of the reactor. The sensitivity of the components of the PRD to the geometrical representation in one-dimension was noted by Meneley and Beitel⁵ in a study of the EBR-II temperature coefficients with both one- and two-dimensional codes. The particular assumptions made in representing EBR-II in a one-dimensional model had so great an effect on the value of the PRD that the analysis was suspect for applicability. Another consideration in selecting the model was the availability of input data, primarily temperatures. The temperatures of the three material components (fuel, sodium, and steel) were available for the six rows of core and upper reflector/blanket regions and for the inner and outer radial reflector/blanket. The availability of temperature data strongly influenced the regional representation and the neutronic calculations. A two-dimensional SNARG-2D code⁶ in r, z geometry was selected for the analysis of the PRD. The calculations were run using an S_n order of two and cross-section Set No. 23806.⁷ The outer iterations converge in a well-behaved manner. No oscillatory behavior was ever observed in obtaining flux convergence to a limit of 1×10^{-6} in 30-90 min. The values of the components of the PRD were obtained by comparing the eigenvalues from successive flux-convergence calculations. The base case

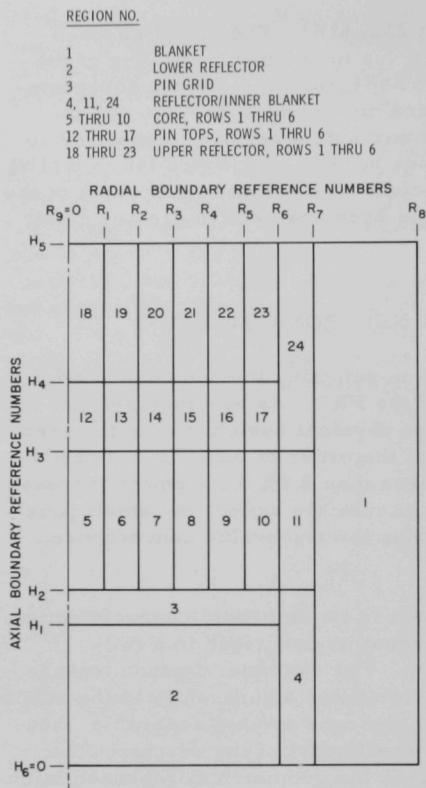


Fig. 2. Regional Representation of EBR-II for Two-dimensional (r, z) Calculations

A. Sodium in the Core (Case A)

The density of the sodium in the core (regions No. 5-10) changes as the temperature increases from 700°F to the values given in Table I for these six core regions at 45 MWt. Sodium in the core is present as flowing

for the study was a zero-power condition at a uniform 700°F. Succeeding calculations were performed with the appropriate material at the temperatures corresponding to 45-MWt operation. The PRD for the material was then obtained from the difference in the eigenvalues between the base case and the case in which that material was at its temperature corresponding to 45 MWt.

The preparation of the input-data specifications for the base case (including the cross-section set and the regional representation of EBR-II shown in Fig. 2) has been discussed in Ref. 4. The regional model for EBR-II allows for an accurate description of the physical changes with increases in power and also for the full use of the available temperature data.

III. PHYSICAL MODEL FOR COMPONENTS OF THE PRD

The components of the PRD will be referred to alphabetically in this discussion. Use of the term "Case" represents the calculation of the components.

TABLE I. Temperatures (°F) by Material and Region in Runs 16, 24, 25, 26, 27, and 27' of EBR-II

Region	Runs 16, 24, and 27'			Runs 25, 26, and 27			Region	Runs 16, 24, and 27'			Runs 25, 26, and 27		
	Fuel	Steel	Sodium	Fuel	Steel	Sodium		Fuel	Steel	Sodium	Fuel	Steel	Sodium
1	720	720	720	720	720	720	11	800	772	770	-	730	730
2, 3, 4	-	700	700	-	700	700	12, 18	-	853	853	-	846	846
5	926	822	776	914	813	773	13, 19	-	849	849	-	844	844
6	918	820	775	911	814	772	14, 20	-	858	858	-	856	856
7	917	821	778	912	817	778	15, 21	-	885	885	-	886	886
8	921	832	792	922	833	793	16, 22	-	896	896	-	904	904
9	911	835	798	919	837	802	17, 23	-	865	865	-	886	886
10	874	811	782	896	826	793	24	850	850	850	-	760	760

coolant, as a thermal bond between the fuel and the cladding, and as stagnant sodium between subassembly cans. Within each subassembly, temperature variations exist for the coolant, the bond, and the stagnant sodium. The sodium temperatures also vary among the different types of subassemblies within a core region at 45 MWt. The temperatures in Table I are average values of all the sodium in all the subassemblies of a given region.

As the bond sodium expands upward with an increase in temperature, the sodium level rises over the fuel pin. The density change of bond sodium in the core region is calculated; however, the change in sodium height over the core region is ignored as being a small reactivity effect.³

B. Sodium in the Upper Reflector (Case B)

The PRD attributed to density changes of the sodium in the upper reflector is obtained by first calculating the total PRD attributed to density changes of sodium in the core and upper reflector and then subtracting the previously calculated PRD of the core sodium (see Section A above). Thus, the density change of the sodium in both the core and the upper reflector is calculated, based on the bulk temperatures of sodium in the six core regions and twelve upper-reflector regions. The assumptions inherent in using a bulk sodium temperature in the upper reflector are the same as they were in calculating the PRD of the core sodium. No changes occur in the volume fractions or dimensions of the materials.

C. Sodium in the Inner-reflector/Blanket Region (Case C)

The PRD component resulting from density change of the sodium in the inner reflector is added to the PRD components previously calculated to obtain a total PRD for sodium in the core and in the upper- and inner-reflector regions. Subtracting the PRD component for the core and upper reflector from this total yields the PRD component for the sodium in the inner-reflector region. An average bulk-sodium temperature is available for Rows 7 and 8 for three axial regions: lower reflector (No. 4), core (No. 11), and upper reflector (No. 24). Particularly in the case of a steel reflector (rather than a depleted-uranium blanket), large radial temperature gradients occur in the sodium. However, the use of bulk temperatures in these regions does not introduce a serious error, because the sodium component at this location has a low worth.

D. Sodium throughout the Reactor (Case D)

Adding the density change of sodium in the outer radial blanket to those density changes discussed in Section C above, permits the total reactivity defect caused by the sodium density change in EBR-II to be calculated. In these calculations, no temperature change of sodium is assumed in the

reflector or blanket regions below the core. However, in the earlier loadings (such as Run 16), the blanket region below the core contained depleted uranium that supplied a small amount of heat to the coolant passing up the subassembly. In all the other loadings, the depleted uranium was replaced with steel, which does not generate heat significant enough to be included in the calculations. The temperature below the core is assumed, in all cases, to be 700°F, even though a small error was introduced in calculating Run 16.

E. Fuel Expansion (Case E)

The fuel is assumed to expand axially according to a calculated fuel temperature for the core regions (No. 5-10). Radial expansion of the fuel is allowed only up to the cladding wall, but is not considered when it would result in a radial expansion of the subassembly. The radial expansion of the fuel pin to the cladding wall is not reflected in the atom densities of the fuel, because the pin is homogenized within the subassembly. The expulsion of the sodium bond from between the fuel and the cladding is ignored, and Doppler and self-shielding changes are not considered. The oxide fuel contained in an experimental subassembly is assumed to expand as much as the driver fuel within the same region. The new length of the fuel pin in each core region is calculated by the following relationship:

$$l_1 = l_0(1 + \alpha \Delta T), \quad (1)$$

where

l_0 and l_1 = initial and final lengths, respectively,

α = linear-expansion coefficient of the fuel,

and

ΔT = fuel temperature change between 0 and 45 MWt.

Because the value of ΔT is slightly different for the six core regions, the upper boundary of Regions 5-10 also would be slightly different. Since the neutronic code is not capable of representing this variation in core height, a uniform core height is obtained by a linear average of the various fuel heights in the six core regions. Effects of burnup, fabrication techniques, impurities, phase changes, etc., are not considered in the expansion coefficient. The density of the fuel is inversely proportional to the core height, so that the total atoms of fuel within the core regions are preserved.

F. Axial Expansion of Steel (Case F)

The power-reactivity decrement caused by expansion of the steel in EBR-II is divided into two components: that caused by axial expansion, and

that caused by combined axial and radial expansion. The idealized physical situation for which the axial-expansion component is calculated is one in which only the steel is at a temperature corresponding to 45-MWt operation, and the steel subassembly cans do not touch their neighbors. Thus, there are no radial dimensional changes. In the axial direction, the core height remains the same, since the temperature of the fuel pin is unchanged. However, the steel in the core region does expand, and this expansion is represented by a change in density of the steel. As was assumed with the other material, all the steel in the region is also assumed to be at the same temperature, although the fuel cladding in the core region is at a higher temperature than is the hex can of the subassembly. However, this difference has been recognized as one of the weaknesses of representing the system and was accepted as such. The steel in the six core regions and that in the radial blankets expand to different heights. The practical considerations in applying these codes to EBR-II require that all the fuel top regions (No. 12-17) and all the upper reflector regions (No. 18-23) have the same boundary. The boundaries for these regions are obtained by averaging the new heights of the individual regions. The density of the steel in the regions above the core is corrected by the ratio of the old height to a new height, so that the total atoms of steel are preserved. Although the temperature increase in the radial blankets is less than that in the upper reflector, the respective heights of the inner and outer radial-blanket regions are assumed equal to the height of the upper-reflector region above the core. Again, this is one of the approximations that must be accepted because of the practical limitations of the neutronic code. In the radial-blanket regions, the densities of the depleted uranium and steel are corrected so that the total amount of material remains constant after the new heights of the regions (No. 1, 4, 11, and 24) are established.

G. Combined Radial and Axial Expansion of Steel (Case G)

The physical model for the combined radial and axial expansion assumes that the subassemblies throughout the core are in contact with their neighbors at 700°F. As the temperature of the steel increases with power, the steel expands both radially and axially; no restraints are assumed for either expansion. At 45 MWt, the final radial dimension of the region is determined by

$$\Delta r_1 = \Delta r_0(1 + \alpha \Delta T), \quad (2)$$

where

Δr_1 and Δr_0 = final and initial thicknesses of radial regions, respectively,

α = linear-expansion coefficient of steel,

and

ΔT = regional temperature change along axial midplane of the reactor.

The atom densities of the steel, fuel, and depleted uranium in each region are assumed to be inversely proportional to the volume of the region. This assumption conserves the total number of atoms of these materials in each region, except for the steel in the core. The sodium density does not change for this component. The volume fraction of all materials again remains constant on operation from 0 to 45 MWt.

H. 45-MWt Operation with No Radial Expansion (Case H)

This case is similar to the one for steel expansion with no radial expansion, but includes the effects of temperature increases in the fuel and sodium. Therefore, it is a combination of components described under Sections D, E, and F above. This component of the PRD represents the physical changes from 0 to 45 MWt without bowing. (Adding the appropriate radial motion, which is nonlinear with power, represents the situation corresponding to the total PRD.) The densities of the steel and of the fuel are corrected for the axial expansion, and the sodium density changes in the same ways as described in Section D above.

I. 45-MWt Operation with Radial and Axial Expansion (Case I)

The conditions considered here are the sum of those described in Sections D, E, and G above. The physical changes simulated by this component are those predicted for the third stage of the bowing phenomena. The fuel and all the sodium are at the temperatures corresponding to full power, and the steel expands in both the radial and axial directions in accordance with the temperature increases along the vertical and horizontal centerlines. As described in Section G, with radial expansion the reactor is assumed to be a rigid structure at 700°F. The appropriate changes in the density of the materials are made in the same manner as for the cases described in Sections D, E, and G.

IV. PREPARATION OF INPUT DATA FOR NEUTRONIC CODES

During the earlier calculation of the PRD,⁸ many errors were found in preparing the input data for the neutronic codes. These errors consisted of round-off errors, inconsistencies in the calculation from case to case, and miscalculated data or mispunched data-processing cards. Because the changes in the system for the study of the PRD are very small, errors are easily made, but difficult to discover. This situation led to the development of a computer code that systematically prepares the input data for the

SNARG-2D code. The ASPIRN code was specifically developed to handle the preparation of data for the PRD study, using the representation of EBR-II shown in Fig. 2. The basic function of the ASPIRN code is to make the appropriate changes in the dimensions of the reactor region, the densities of the materials, and the compositions of the particular loading, and to punch the SNARG-2D input cards for the calculation of the given component of the PRD.

The input data consist, in part, of the material temperatures by region and the regional dimensions for the base case at 700°F and 45-MWt power. The material temperatures are given for loadings with a depleted-uranium blanket (Runs 16, 24, and 27') and for loadings with a steel reflector (Runs 25, 26, and 27) in Table I. Although the core loadings differ for each run, reorificing of the coolant flow minimizes the changes in temperatures among the loadings with the same type of material in the inner-reflector/blanket region. The use of one set of temperatures for three loadings does not introduce a significant error in the calculations.

Table II presents the dimensions for the regions at 700°F shown in Fig. 2. The dimensions at 45 MWt are calculated using a steel-expansion coefficient of $1.0 \times 10^{-5}/^{\circ}\text{F}$, a fuel-expansion coefficient of $9.2 \times 10^{-6}/^{\circ}\text{F}$, and the temperature increments given in Table I. The ASPIRN code uses the following equation to calculate the sodium density (ρ) at the temperatures of interest:

$$\rho = 1.1173 - 0.000159T \text{ (g/cm}^3\text{)}, \quad (3)$$

where

T = temperature in °F.

TABLE II. Radial and Axial Dimensional Boundaries for the Regional Representation of EBR-II at 700°F

Radial Boundary	Radius, cm	Axial Boundary	Height, cm
R_1	3.116	H_1	40.163
R_2	8.191	H_2	50.377
R_3	13.581	H_3	84.867
R_4	18.952	H_4	94.709
R_5	24.335	H_5	135.244
$R_6^{(a)}$	-		
R_7	40.505		
R_8	78.608		

(a) R_6 is 26.982 cm for Run 16, 28.041 cm for Run 24, 29.227 cm for Run 25, and 29.772 cm for Runs 26, 27, and 27'.

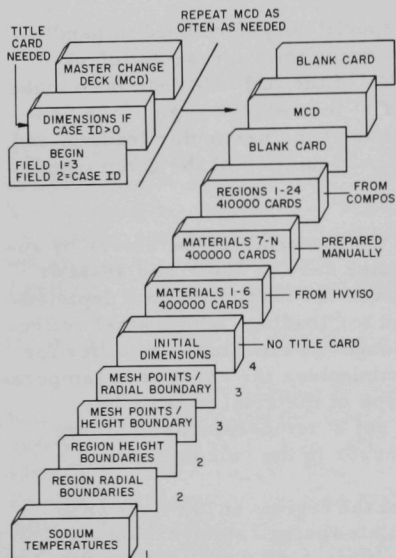


Fig. 3. Structure of ASPIRN Input Deck

The arrangement of data cards for the ASPIRN code is presented pictorially in Fig. 3. The ASPIRN code requires the following input data: sodium temperatures by region, initial regional radial boundaries, initial regional axial boundaries, mesh points per axial boundary, mesh points per radial boundary, initial dimensions of regions, and a description of the materials and their compositions. The data are followed by the Master Change Deck (MCD) that performs the calculations. The data put in before the MCD are identical to the data used for the base case (700°F), much of which were prepared by other computer codes (HVYISO and COMPOS).⁴ With the appropriate designations in the MCD, the input deck to the SNARG code can be prepared by the ASPIRN code. Wherever the calculation of the component requires a new dimension, such as fuel expansion and/or steel expansion, the ASPIRN code reads

in the new dimension and calculates the quantities given in Table III. The MCD contains the directions for changing the density of each material and composition read as input; Table IV gives the specifications for making these changes. After the appropriate alterations have been made in the base case,

TABLE III. Quantities Used in Correcting Material Density for Expansion in the PRD Components

MCD Quantity	Table Entry
1	Volume ratio
2	Area ratio
3	Height ratio
4	Overall height ^a ratio, selected regions
5	Sodium fraction changes
6	Overall height ratio x area ratio, selected regions

^aOverall height refers to heights extending over two regions.

TABLE IV. Punched-card Specifications for Changing the Density of Material and/or Composition in ASPIRN Code

Columns	Code Name	Code	Description
1-6	TYPE	1	A material is to be changed.
		2	A composition is to be changed.
7-12	COMA	n	Material or composition number; n must be \leq the largest material or composition number.
13-18	MANU	m	Material or nuclide number, depending on COMA. Materials occur in compositions, and nuclides occur in materials.
19-24	CHANGE	c	Change fraction $1 \leq c \leq 6$ according to Table III.
25-30	REGION	r	If TYPE = 1, the region in which the change is to be made must be specified.

the base case. Any changes in these cards that normally do not occur in PRD calculations would be made manually.

The changes in the sodium density are made by the ASPIRN code, which compensates for the temperature of the sodium in a particular region, and using the linear relationship between sodium density and temperature given in Eq. 3, calculates the ratio of sodium density at the new temperature relative to that at 700°F. Changes in atom densities for steel and fuel caused by expansion are accounted for by multiplying the density of the fuel or steel by the ratio of the area, height, or volume at the 45-MWt operating temperature relative to that at 700°F. Table V outlines the calculations performed by the ASPIRN code in preparing the new materials and compositions for each of the nine components of the PRD. Figure 2 gives the region numbers referred to in Table V.

TABLE V. Outline of Calculations Performed on Base Case to Obtain Components of the PRD

Case	Material	Region No.	Corrections for	Comments
A	Sodium	5-10	Density	Sodium in core
B	Sodium	5-10, 12-23	Density	Sodium as in Case A plus pin tops, upper reflector
C	Sodium	5-24	Density	Sodium as in Case B plus inner blanket (Rows 7 and 8)
D	Sodium	1, 5-24	Density	Sodium as in Case C plus outer blanket
E	Fuel	5-10	Volume ratio	Fuel expansion
F	Steel	1, 18-23	Volume ratio	Steel, axial expansion
	Steel	5-17, 24	Overall height ratio x area ratio	
G	Fuel	5-10	Area ratio	Steel, radial and axial expansion
	Steel	1-4, 18-23	Volume ratio	
		5-17, 24	Overall height ratio x area ratio	
	Fuel blanket ^a	4, 11, 24	Area ratio	
H	Sodium	1, 5-24	Density	45 MWt without radial expansion
	Fuel	5-10	Volume ratio	
	Steel	5-17, 24	Overall height ratio x area ratio	
	Steel	1, 18-23	Volume ratio	
I	Sodium	1-24	Density	45 MWt with radial expansion
	Fuel	5-10	Volume ratio	
	Steel	5-17, 24	Overall height ratio x area ratio	
	Steel	1-4, 18-23	Volume ratio	
	Fuel blanket ^a	1-4, 11, 18-23	Area ratio	
	Fuel blanket ^a	24	Volume ratio	

^aDepleted-uranium "fuel" in blanket.

the new input data are punched into cards in the proper format for the SNARG-2D code. The only remaining cards to be provided for the SNARG input are the job-control cards and the code-dependent cards. The cards that designate composition assignments to regions, the type of calculation performed, and means of obtaining the initial fluxes are copied directly from

The input specifications obtained from the ASPIRN code were compared with those previously calculated manually and run in a series of SNARG-2D calculations. The ASPIRN code produced the correct input deck for calculating each component and also provided more significant figures in the input specifications than had been available previously.

V. RESULTS AND DISCUSSION

A. Major Features of Runs 16, 24, 25, 26, 27, and 27'

The significant features of the loadings for which the PRD was calculated are presented in Table VI and discussed here.

TABLE VI. Description of EBR-II Core Loadings for Runs 16, 24, 25, 26, 27, and 27'

Item	Run Number					
	16	24	25	26	27	27'
Number of subassemblies in core	75	81	88	91	91	91
Composition of Rows 7 and 8	Depleted uranium	Depleted uranium	Steel	Steel	Steel	Depleted uranium
Fuel type	Mark I	Mark IA	Mark IA	Mark IA	Mark IA	Mark IA
Axial blanket						
Material	Depleted uranium	Steel	Steel	Steel	Steel	Steel
Design (pin = p; triflute = t)	75p	81p	50p/13t	33p/31t	16p/45t	16p/45t
Number of experiments in core	5	9	11	13	16	16

Run 16 was the only run in which Mark-I fuel predominated in the core. Also, it contained the fewest number of subassemblies in the core of the runs considered here. Of the six runs considered in this report, only Run 16 contained depleted uranium in the axial blankets.

Run 24 had a slightly larger core than did Run 16 and contained more experiments. The loading was fueled primarily with Mark-IA fuel, and the axial blankets were replaced with a steel reflector of the pin design.

In Run 25 the most significant difference was the addition of steel reflector subassemblies in the inner-blanket region. This loading had a slightly larger core in which additional experimental subassemblies were present. Axial reflectors of triflute design were introduced into this core; however, the pin design still predominated.

Run 26 was the first core loading in which the full six rows of EBR-II contained core subassemblies. Half of the core subassemblies had axial reflectors of the pin design, and half of the triflute design. More experimental subassemblies were added in Run 26.

Run 27 contained the largest number of experimental subassemblies within the core region of any loading up to that time. Most of the core subassemblies had reflectors of the triflute design. In other respects, the loading for Run 27 was similar to that for Run 26.

Run 27' was a fictitious loading, identical to Run 27 except for two alterations. First, the steel reflector was replaced with a depleted-uranium blanket; second, two fully loaded subassemblies replaced two half-loaded subassemblies to achieve the proper k_{eff} .

B. Presentation of Results

Table VII presents the values of the nine components of the PRD from 0 to 45 MWt for the six loadings of EBR-II. Table VIII gives the temperature and expansion coefficients applicable for each of the six loadings.

TABLE VII. Values of PRD Components (Δk) for Runs 16, 24, 25, 26, 27, and 27'(a)

Component	Run Number					
	16	24	25	26	27	27'
Sodium in core	44.7	40.7	43.6	40.8	41.7	39.3
Sodium in upper reflector	29.6	30.9	40.7	40.1	41.3	37.5
Sodium in inner reflector	5.9	7.2	3.6	3.2	3.4	5.6
Total sodium	80.4	79.0	88.2	84.5	86.7	82.4
Fuel	44.6	43.6	42.3	41.5	42.0	44.0
Steel expansion						
Axial	8.7	9.1	12.4	17.9	17.3	10.9
Axial and radial	119.6	118.2	122.0	129.0	132.7	99.6
Total decrement						
No radial expansion	135.2	138.1	152.1	147.7	148.1	141.3
With radial expansion	255.3	250.3	255.7	253.9	265.9	244.0

(a) All values for Δk in the table have been multiplied by -1×10^5 .

TABLE VIII. Temperature and Expansion Coefficients for Runs 16, 24, 25, 26, 27, and 27'

	Run Number					
	16	24	25	26	27	27'
Temperature Coefficient, $(-\Delta k/k)/^\circ\text{F} \times 10^{-5}$						
Sodium in core	0.494	0.465	0.481	0.462	0.453	0.451
Sodium in upper reflector	0.160	0.189	0.223	0.222	0.225	0.214
Sodium in inner reflector	0.084	0.103	0.120	0.107	0.113	0.080
Fuel	0.211	0.206	0.200	0.196	0.199	0.218
Expansion Coefficient, $-1/\text{in}/^\circ\text{F}$						
Fuel	0.646	0.650	0.631	0.619	0.627	0.656
Steel, radial	3.2	3.4	3.3	3.3	3.4	3.5

C. Discussion of the Components of the PRD

Since several changes were made after each loading considered, a simple cause-and-effect relationship is not easily established between one loading change and a change in the PRD or a component of the PRD. Moreover, the possible effects of burnup, control-rod position, and local changes that are not reflected in the homogenization of a region were not investigated in this report. Another complication in isolating a causal relationship arises from reorificing the coolant flow each time experimental and other special subassemblies were added to the core. Thus, many

factors are involved in comparing the results of one loading with those of another. Before the results are analyzed, it should be remembered that the values of the components of the PRD and the total PRD represent very small quantities and in some cases approach the limit of accuracy of the computational method. The limitations of the study are presented here, so that the conclusions in the following paragraphs can be seen in the proper perspective.

In the individual component or the total PRD in the six cases studied, there are no changes that explain the decrease in the measured PRD in going from Run 24 to Run 25. This finding is not surprising, because that decrease has been attributed to nonlinear components. Moreover, no component exhibits a large trend with the various changes in loading for EBR-II, and the total PRD's for Cases H and I (Section III) are of the same magnitude for each of the six loadings studied. The following paragraphs discuss the trends of the individual components in terms of changes in the loading of EBR-II.

1. Sodium in the Core

The value of the PRD for sodium in the core region decreases as the core size increases. This is seen by comparing Run 16 to Run 24 and Run 25 to Run 26. The compositional change of the inner-blanket region from steel to uranium increases the PRD of sodium in the core. This is seen by comparing the values for Runs 24 and 25 (40.7 versus 43.6) and Runs 27' and 27 (39.3 versus 41.7).

2. Sodium in the Upper Reflector

The reactivity change caused by a change in sodium density in the upper reflector increases through Runs 16 to 27, which suggests an increase with increasing core size. This increase may be related also to changing the design of the upper reflector. As reflectors with the trifluted design are added to the reactor, the volume fraction of sodium in the upper reflector decreases and may influence the value of the PRD. One of the largest changes in a component of the PRD from one run to the other is seen by comparing the value of the PRD for sodium in the upper reflector in Run 24 to that in Run 25. A significant, but smaller, change is between Runs 27 and 27', which are identical except for the composition of the inner-blanket region. That region appears to play a significant role in the value of the PRD of sodium in the upper reflector, but the reason for this is not clear from the information available.

3. Sodium in the Inner Reflector

The value of the PRD for the sodium component in the inner reflector is largest for the loadings with depleted uranium in the region,

but the value of this PRD component is too small to draw any conclusions concerning the effect of core size. The inner-blanket region has the same volume fraction of sodium in the steel as in the depleted-uranium subassemblies.

4. Sodium in the Reactor

The remaining component of the sodium that has not been investigated is that of the sodium in the outer blanket. However, the temperature rise of this sodium is only 20°F from 0 to 45 MWt, and the reactivity importance of the changes in the outer blanket is small. Therefore, the value of the PRD for the sodium in the outer blanket is so small that it cannot be calculated within the accuracy of the convergence of the neutronic code. The value of the PRD for sodium throughout the entire reactor is approximately the same for all six runs considered. Lack of a significant variation in the component of the total sodium results from the cancellation of the trends of the individual components when totaled. Although the PRD for the core sodium decreases with core size, that for the upper-reflector sodium increases. The presence of steel in the inner-blanket region causes a lower PRD for sodium in that region but a larger PRD for the sodium in the upper reflector.

5. Fuel Expansion

The value of the fuel component decreases slightly in going from Run 16 to Run 27, but increases when a depleted-uranium blanket surrounds the core (Run 27'). The effect of a blanket change is not seen in comparing the results from Runs 24 and 25. No strong effects are seen in the six values of the fuel component of the PRD. However, the effects of burnup, which may change the conductivity or the expansion coefficient, and those of phase change on the expansion coefficient have not been considered here.

6. Axial Expansion of Steel

Although the reactivity decrement resulting from axial expansion of the steel is not large, it shows one of the more distinct trends. The presence of the steel reflector in the inner-blanket region increases the value of the decrement, as can be seen from the values for Runs 25, 26, and 27. The placement of depleted uranium in the inner-blanket region in Run 27' results in a decrease of 6 lh.

7. Combined Radial and Axial Expansion of Steel

A substantial variation in the decrement caused by radial and axial expansion of steel is seen for the six runs. However, an explanation of these variations is not apparent. For example, the value for Run 27' appears to be much lower than that for the other runs without any apparent

reason. Although the presence of the depleted-uranium blanket lowers the value of the decrement, the difference observed by comparing Runs 27 and 27' was not expected.

D. Discussion of the Temperature and Expansion Coefficients

As was mentioned in Section IV, one set of temperatures was used for all loadings having a full depleted-uranium blanket, and one set of temperatures was used for all loadings having a steel reflector in the inner blanket. Temperature coefficients are very useful in comparing the reactivity effects of loadings having different regional temperatures. Table IX lists the average temperatures of the sodium in the core, upper reflector, and inner-blanket/reflector regions and of the fuel in the core. That table also gives the magnitudes of the expansion of the core radius and of the fuel height.

TABLE IX. Average Material Temperatures and Expansions for
Runs 16, 24, 25, 26, 27, and 27'

Item	Run Number					
	16	24	25	26	27	27'
Average temperature of sodium in core, °F	791	787	792	792	792	787
Average fuel temperature, °F	811	811	811	811	811	811
Average temperature of steel in core, °F	830	825	828	828	828	825
Expansion of core radius, cm	0.0347	0.0349	0.0364	0.0370	0.0370	-
Average temperature of sodium in upper reflector, °F	881	876	884	884	884	876
Average axial fuel expansion, cm	0.069	0.067	0.067	0.067	0.067	0.067
Average temperature of sodium in inner reflector, °F	~775	~775	~730	~730	~730	~775

1. Sodium in the Core

The temperature coefficient of the sodium in the core showed two trends, which are similar to those seen in the PRD for the component. One trend is a decrease in the temperature coefficient with increasing size of the core. For the runs with a full depleted-uranium blanket (i.e., Runs 16, 24, and 27'), the value of the sodium coefficient decreases from 0.494 to 0.451 as the core size increases from 75 to 91 subassemblies. The same trend in the temperature coefficient in the sodium in the core is seen for loadings with a steel radial reflector (i.e., Runs 25, 26, and 27). However, the changes in the sodium coefficient seem large in relationship to the small change in the core size of 88 to 91 subassemblies. The second trend observed is that the temperature coefficients for all the loadings with

steel reflectors are greater than those with a depleted-uranium blanket. However, because of the small differences in the coefficient for Runs 27 and 27', it is not possible to conclude that the material in the inner blanket has a strong effect on the sodium coefficient.

2. Temperature Coefficient of Sodium in the Upper Reflector

The temperature coefficient of sodium in the upper reflector tends to increase with increased core size, which is opposite to the behavior of the sodium coefficient in the core region. For the loadings with a uranium blanket, the values vary from 0.160 for a 75-subassembly core to 0.214 for a 91-subassembly core. The effect of the material in the inner-blanket region is more pronounced on the temperature coefficient in the upper reflector than on that in the core. The presence of a uranium blanket lowers the temperature coefficient for the upper-reflector region. This observation is particularly apparent in comparing Runs 27 and 27', where the difference between the values of the temperature coefficient is large enough to be meaningful.

3. Temperature Coefficient of the Fuel

The temperature coefficient of the fuel is fairly uniform for the six runs and varies only $\pm 5\%$ from the average value. There does not seem to be any noticeable trend of the fuel-temperature coefficient with core size. The value of the coefficient decreases from Run 16 until Run 26, but then increases in Runs 27 and 27'. The coefficient is slightly larger for loadings with a uranium blanket; the most noticeable indication of this possible trend is seen by comparing the values for Runs 27 and 27'.

4. Sodium in the Inner Reflector

The sodium-temperature coefficient in the inner-reflector region is greater when the region contains steel rather than depleted uranium. As will be seen in Section VI, the neutronic importance of the inner-blanket/reflector region is greater when a steel reflector is present.

5. Expansion Coefficients of Fuel and Steel

The expansion coefficients of fuel (axial) and steel (radial) show no discernible trends. All fuel-expansion coefficients lie within 3% of the average value, and a $\pm 5\%$ range encompasses the steel coefficients. So many approximations are made in obtaining the expansion coefficients that important reactivity effects are lost, especially those of steel expansion.

E. Internal Consistency of the Calculated Values

The values of the components of the PRD given in Table VII are internally consistent with one another. The sum of the values of the PRD components due to sodium in the core, the upper reflector, and the inner reflector is in close agreement with the value for the total PRD due to sodium throughout EBR-II (Section III.D). This is not a definite proof of internal consistency of the calculations, because the sodium components in the upper and inner reflectors were obtained by subtracting them from a total reactivity defect rather than by calculating them individually. However, since the fraction of the sodium component in the various regions is approximately of the same magnitude in all six runs studied, there probably are no significant errors in the calculations of these components. A more meaningful indication of internal consistency of the values is obtained by comparing the components of the total decrement with the sum of the individual material components. This is done by adding the components for sodium, fuel, and expansion of the steel and by comparing the sum with the total decrement for Cases H and I of Section III. For no radial expansion, the sum of the individual components (Sections III.D, E, and F) is slightly lower than the total decrement (Section III.H). The largest difference is about 12%, whereas most differences are of the order of 3-5%. Although the deviation of 12% in Run 25 has not been explained, the component for the axial expansion of steel is suspected. Closer agreement is seen between some of the individual components (Sections III.D, E, and G) and the total decrement with radial expansion (Section III.I). In this case, the largest deviation is about 5% (again in Run 25). With one exception, the individual components of sodium, fuel, and steel expansion are in the same proportion for all loadings. The one exception is the combined radial and axial steel expansion for Run 27', which is about 15% lower than in all other runs. Besides indicating the internal consistency of the calculations and an absence of large errors in the input quantities, the agreement between the sum of the individual components and the total decrement indicates that the reactivity effects are additive within a few percent. In other words, the fuel-expansion coefficient is not greatly affected by the temperature of the sodium in the core or reflector regions. The same appears to be true for the other components.

The values of both the total and the individual components of the PRD are very small numbers that are obtained from differences between numbers of the order of 1.0. Thus, even with a relatively tight convergence of 1×10^{-6} , some error may be introduced into the results by variations in the convergence of the neutronic code. A prohibitive amount of computer time would be required to obtain the degree of convergence needed to eliminate this source of error. Other approximations, representing the system by a neutronic model, probably contribute errors of the same order of magnitude as those caused by convergence of the eigenvalue.

VI. FURTHER INVESTIGATION OF RADIAL MOTION

Although the linear components of the PRD make up a sizable portion of the total PRD, their analysis does not explain the change in the total PRD with a change of the inner-blanket material. A nonlinear effect, caused by bowing of subassemblies, changes the total PRD. Radial motion of the subassemblies resulting from bowing produces the reactivity effects of the nonlinear component. Because of the importance of radial motion to the PRD, further investigation was conducted into the reactivity effects of inward and outward movement of the subassembly.

During the investigation, the distance between the subassemblies in the core and blanket regions was theoretically increased and decreased under isothermal conditions at 700°F to represent expansion and compaction, respectively. The reactivity worths were calculated for uniform movement of the six rows of core subassemblies, the two rows of inner-reflector subassemblies, and all rows of depleted-uranium blanket subassemblies. The calculations were performed for Runs 16, 24, 25, and 26. To obtain each reactivity worth, two eigenvalue calculations were performed in addition to the base case for each run. The expansion coefficient for the core was obtained by calculating the eigenvalue for increases of 1 and 2 mils between the core subassemblies at 700°F while the clearance between the remaining subassemblies was kept the same. The change in the eigenvalue for the two calculations was proportional to the change in the clearance between the subassemblies. The same method was used for calculating the other expansion and compaction coefficients. Table X shows the results.

TABLE X. Isothermal Expansion and Compaction Coefficients of the Core, Blanket, and Reflector for Runs 16, 24, 25, and 26

Run	Expansion Coefficient, -Ih/mil		Compaction Coefficient, -Ih/mil	
	Core	Blanket/Reflector	Core	Blanket/Reflector
16	3.13	0.10/N.A. ^a	2.73	0.11/N.A. ^a
24	2.73	0.11/N.A. ^a	2.61	0.11/N.A. ^a
25	2.60	N.C. ^b /0.39	2.53	0.04/N.C. ^c
26	2.50	N.C. ^b /0.40	2.55	0.03/N.C. ^c

^aN.A.--not applicable; no reflector region present.

^bN.C.--not calculated; approximately equal to compaction coefficient (-0.03 to -0.04 Ih/mil).

^cN.C.--not calculated; approximately equal to expansion coefficient (-0.4 Ih/mil).

One of the most evident effects of core size is in the values of the expansion coefficient, which decrease from -3.13 Ih/mil for a 75-subassembly core (Run 16) to -2.50 Ih/mil for a 91-subassembly core (Run 26). The compaction coefficient also was smaller for the larger cores, but the effect was not as pronounced. The expansion and compaction

coefficients for the steel reflector (Runs 25 and 26) are much larger than those for depleted uranium in the entire radial blanket (Runs 16 and 24).

These data are very useful in determining the consistency of the results obtained in the analysis of the linear components. The total PRD is the sum of all linear components plus the nonlinear component caused by radial movement produced by subassembly bowing. The value of the nonlinear portion of the PRD was obtained by subtracting the linear portion from the total. The reactivity change caused by bowing with increasing power can be converted into a change of radial position of the subassembly

by using the data in Table X. Although this technique will not give an accurate or perhaps even a unique description of the subassembly positions during an increase in power, it yields a reactivity change due to radial motion of the subassemblies of the correct magnitude and thus adds confidence to the data on the linear components of the PRD. Figure 4 provides an example of how this technique is applied. For the purposes of this analysis, the PRD values between 0 and 45 MWt are plotted as a series of three straight lines. (The PRD values are usually plotted as a curve with a smoothly varying slope.¹) The slopes of the lines in Fig. 4 represent a constant power coefficient over the length of the line. The power coefficient due to the linear components of the PRD for Run 24 is obtained by dividing the total decrement

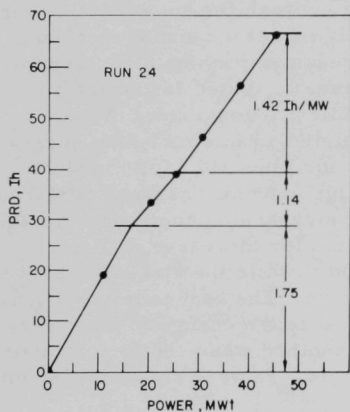


Fig. 4. PRD Curve for Run 24 Presented as Three Linear Segments

without radial expansion ($1.381 \times 10^{-3} \Delta k$, from Table VII) by the power change (45 MWt) and converting the result to Ih/MWt by the relationship $1\% \Delta k = 425 \text{ Ih}$. The procedure yields a linear power coefficient of -1.30 Ih/MWt . The nonlinear component of the PRD is then obtained by subtracting the linear component of -1.30 Ih/MWt . The approximate nature of this procedure is seen in that the nonlinear components are assumed to be linear over a substantial power range (~ 10 -20 MWt). Table XI lists the PRD coefficients for the total PRD and for the nonlinear components over three power ranges. The radial motion of the core subassemblies is calculated by dividing the reactivity change over a segment of the power due to nonlinear effects by the appropriate coefficients (column four) in Table X. The change in the radial position of the core subassembly due to thermal expansion is also calculated for the three power segments.

This approximate representation* gives a consistent picture for radial motion. From 0 to 16.5 MWt, the model predicts an outward movement

of 2.7 mils while the subassemblies expand thermally 0.8 mil. This leaves a net clearance of 1.9 mils between core subassemblies. In the middle power range, the core and inner-blanket regions are predicted to compact by 0.8 mil, and thermal expansion adds another 0.7 mil to the closing of the gaps between the subassemblies. At the upper power limit of the second stage, the clearance between the subassemblies is predicted by this approximate model to be 0.4 mil.

TABLE XI. Predicted Pattern of Radial Motion of Subassemblies during an Approach to Power

Power Range, MWt	Total Power Coefficient, -1h/MWt	Nonlinear Coefficient, -1h/MWt	Movement of Core Subassembly, mils	Thermal Expansion, mils	Clearance between Subassemblies at Upper Power Limit, mils
0-16.5	1.75	0.45	2.7 (out)	0.8	1.9
16.5-22.5	1.14	-0.16	0.8 (in)	0.7	0.4
22.5-45	1.42	0.12	0.8 (out)	a	0.0 ^a

^aReactor assumed to be a compact, rigid structure.

Although this model did not predict the full compaction of the core at the power where compaction changes to expansion, it did come fairly close and also predicted a motion that is physically possible and realistic.

A similar analysis, performed on the PRD data obtained from Run 25, predicted that the subassemblies in the core would actually compact more at 45 MWt than at zero power. This prediction is generally consistent with the examination of subassemblies removed from EBR-II after Run 25. This examination gave evidence that the subassemblies may have been permanently deformed to a smaller dimension than they had when they entered EBR-II.⁹

Although this technique is very sensitive to the slope of the line drawn that represents the three stages of the power-reactor decrement, it gives results that are consistent with the results of measurements when the values for the linear components of the power coefficient are used.

VII. OTHER RELATED REACTIVITY EFFECTS

A. Loss of Fuel-expansion Coefficient in Some Fuel Subassemblies

As additional oxide-fueled experimental subassemblies are added to EBR-II, the question of possible changes in the fuel-expansion coefficient arises. Measurements of the PRD of the Rapsodie¹⁰ reactor indicated that the oxide fuel loses its expansion coefficient under irradiation in the reactor.

The influence of oxide-fueled experimental subassemblies on the fuel-expansion coefficient was studied for the simplified, but realistic, loading of EBR-II described in Table XII. The uranium enrichment of the mixed-oxide experimental subassemblies was set at 59.8 at. % to achieve criticality for this loading. Four calculations were performed to study the expansion coefficient: two cases in which the full core was expanded 0.2 and 0.4 in., and two cases in which all but the structural and oxide-fueled experimental subassemblies were expanded 0.2 and 0.4 in.

TABLE XII. EBR-II Loading for the Study of the Influence of Oxide-fueled Experimental Subassemblies on the Fuel-expansion Coefficient

Type of Subassembly	Total Number of Subassemblies	Row and (Number in Row)
Mark-IA fuel	53	1 (1), 3 (10), 5 (12), 6 (30)
Mark-IA safety	2	3 (2)
Mark-IA control	12	5 (12)
Structural experiment	6	2 (6)
Encapsulated oxide experiment ^a	9	4 (9)
Unencapsulated oxide experiment ^b	9	4 (9)

^a59.8%-enriched UO_2 -25 wt % PuO_2 ; 17.3 vol % fuel, 37.5 vol % steel, 45.2 vol % sodium.

^b59.8%-enriched UO_2 -25 wt % PuO_2 ; 39.0 vol % fuel, 23.7 vol % steel, 37.3 vol % sodium.

These calculations cover the range of situations in which the mixed-oxide fuel is assumed to expand as much as the metal fuel at one extreme and to have no expansion at the other extreme. The results of the calculations, presented in Table XIII, indicate a 17.7% reduction in the magnitude of the expansion coefficient under the most pessimistic situation, that in which the fuel of the experimental subassemblies does not expand. When the expansion coefficients are normalized per kilogram of ^{235}U (equivalent) being expanded, the differences in the results of the four cases become small (~2%). The fuel-expansion coefficient calculated for EBR-II Runs 24-27 is $-1.59 \times 10^{-2} \Delta k / \Delta L$ (in.⁻¹), or about -0.64 lh/mil (see Table VIII).

TABLE XIII. Results of Study of Fuel Expansion with Mixed-oxide Subassemblies

Rows Expanded	Fuel Expanded, kg	Distance Expanded, in.	Reactivity Change, $-\Delta k \times 10^3$	Fuel-expansion Coefficient, $-\Delta k / \Delta L \times 10^5$, in. ⁻¹	$-\Delta k / \Delta L / \text{kg} \times 10^5$
1, 2, 3, 4, 5, 6	~215	0.20	3.224	1.612	7.50
1, 2, 3, 4, 5, 6	~215	0.40	6.458	1.614	7.50
1, 3, 5, 6	~180	0.20	2.646	1.326	7.37
1, 3, 5, 6	~180	0.40	5.314	1.328	7.38

An important finding of the investigation is that the expansion coefficients for these cases are proportional to the amount of fuel expanded and are constant with the distance expanded between 0.0 and 0.4 in. Expanded fuel has the same neutronic importance for the four cases considered and greatly influences obtaining a coefficient proportional to the amount of fuel expanded. The proportionality would not exist between one case in which only the fuel in the core center expanded and another case in which only the fuel at the core edge expanded.

Care must be used in applying the results of the investigation to specific loadings of experimental subassemblies, and the worth of the experimental subassemblies, relative to the driver fuel, must be determined for the actual fuel loading of the experiments and their position in the reactor. If some experimental fuels (such as carbide or metal fuels) are assumed to expand during the approach to full power, the temperature increase and expansion coefficient probably will be different than those of the driver fuel. The quantity that is least sensitive to the particular loading of the experimental subassemblies in the reactor is $-7.5 \times 10^5 \Delta k / \Delta L / g$ of ^{235}U .

B. Reactivity Changes due to Slumping of Fuel Pins

A reactivity effect not directly related to the PRD, but of considerable interest, is that due to slumping of the fuel pins. In the Mark-IA design, the fuel pin occupies ~85% of the volume within the cladding, and the sodium bond occupies the remaining 15%. If the pin melted during reactor operation, the pin would contract axially within the cladding and produce a positive reactivity effect.

The reactivity effect of slumping of the fuel pins in the center subassembly of EBR-II was calculated by comparing the eigenvalues of the Run-25 loading with and without slumping of the fuel pins in the center subassembly. Two models of fuel slumping, designated Problems 1 and 2, were investigated here. In Problem 1, the slumped fuel pins were assumed to occupy the entire volume within the bottom part of the steel jacket. The bond sodium previously between the fuel pin and the jacket was assumed to fill the volume above the slumped fuel pin. Problem 2 differs from Problem 1 in that the bond sodium was assumed to escape into the coolant channel, leaving a void in the region above the fuel pin. Table XIV describes the subassembly, with and without slumping.

The reactivity change caused by fuel slumping is $+56.6 \times 10^{-5} \Delta k$ (24.3 lh) for Problem 1 and $+49.2 \times 10^{-5} \Delta k$ (21.2 lh) for Problem 2. As a rough rule of thumb, the slumping of a fuel pin in the center subassembly position is worth ~1/4 lh, but the reactivity change would be smaller in other subassembly locations.

TABLE XIV. Compositions, Dimensions, and Eigenvalues of an EBR-II Run-25 Subassembly with and without Fuel Slumping

	No Slumping; 700°F Full Core	Fuel Slumped			
		Problem 1		Problem 2	
		Fuel Region	Sodium-bond Region	Fuel Region	Void Region
Length, cm	34.490	29.388	5.102	29.388	5.102
Volume fractions, %					
Fuel	32.631	38.296	0.0	38.296	-
Sodium	47.530	41.865	80.161	41.865	-
Steel	19.839	19.839	19.839	19.839	-
Eigenvalue at 700°F	1.026999	1.027565		1.027491	

VIII. COMPARISON OF CALCULATED AND MEASURED VALUES

Few comparisons of the calculated values of the PRD components with experimental ones are possible because of the difficulty in measuring individual linear components or even a combination of linear components. The total PRD is readily measured, but the linear portion cannot be separated. The nonlinear components have been excluded from two measurements. One is the measurement of fuel-expansion component obtained by constant- ΔT experiments.¹¹ The other measurement, which has been made repeatedly, is that of the isothermal coefficient. Since the isothermal coefficient contains no nonlinear effects, the temperature and expansion coefficients in Table VIII can be used to calculate an isothermal coefficient for the entire reactor.

A value of $-0.95 \text{ Ih}/^\circ\text{F}$ is calculated for Run 25 from the linear components of the PRD; this value is -6% lower than the measured value of $-1.01 \text{ Ih}/^\circ\text{F}$. A value of $-0.404 \text{ Ih}/\text{MWt}$ is calculated for the fuel-expansion component in Run 25, whereas the measured value is $-0.65 \text{ Ih}/\text{MWt}$. Recent information¹¹ has indicated that the linear-expansion coefficient of $9.2 \times 10^{-6}/^\circ\text{F}$ for the fuel, which was used in these calculations, is considerably low, and that the coefficient should be about $13 \times 10^{-6}/^\circ\text{F}$. Increasing the value of the linear-expansion coefficient of the fuel would reduce the discrepancy between the measured and calculated values of both the isothermal temperature coefficients and the fuel-expansion coefficients. A larger fuel-expansion coefficient also would predict a pattern of subassembly movement (as discussed in Section VI) more consistent with that suggested from the analysis of bowing. A larger linear component of the PRD would predict a more compact core at the power where the reactivity effect of bowing changes from positive to negative. The bowing analysis states that the core subassemblies become tightly compacted as the reactivity effect turns positive; however, the calculated linear components predict a clearance of about 0.4 mil between subassemblies.

The data presented here have indicated that the linear components of the PRD are influenced by the changes in core loadings, such as core size and the material in the inner-blanket region. However, changes in the total linear component from one loading to another are small compared to the total PRD. The largest change in the total PRD (between Runs 24 and 25) resulted from a change in the nonlinear components.

An internal consistency is found in the values of the various linear components. The techniques developed for performing the calculations yield reliable, precise results, with little time required for data preparation.

The calculated results have been lower than measured values in the few cases where comparisons are possible. The discrepancy seems to be caused by the assumed values for linear-expansion coefficients, temperature, etc., rather than by the techniques used for calculating the values.

REFERENCES

1. R. R. Smith, T. R. Bump, R. A. Cushman, R. W. Hyndman, F. S. Kirn, W. B. Loewenstein, J. K. Long, J. T. Madell, P. J. Persiani, and W. R. Wallin, *The Effects of an Over-cooled Stainless Steel Reflector on the EBR-II Power Coefficient*, ANL-7544 (May 1969).
2. J. A. DeShong, Jr., *Dynamic Analysis of Liquid-metal-cooled Fast Power Reactors*, ANL-7529 (Jan 1969).
3. L. J. Koch, H. O. Monson, D. Okrent, M. Levenson, W. R. Simmons, J. R. Humphreys, J. Haugsnes, V. Z. Jankus, and W. B. Loewenstein, *Hazard Summary Report: Experimental Breeder Reactor II (EBR-II)*, ANL-5719 (May 1957).
4. J. T. Madell and R. E. Jarka, *Comparison of Various Neutronic Representations for EBR-II Analyses*, ANL-7540 (to be published).
5. D. A. Meneley and J. C. Beitel, Argonne National Laboratory, *Systematic Study of Linear Power Coefficients for EBR-II Project*, private communication (Sept 13, 1967).
6. G. J. Duffy, H. Greenspan, S. D. Sparck, J. V. Zapatka, and M. K. Butler, *SNARG-2D, A Two-dimensional, Discrete-ordinate, Transport-theory Program for the CDC-3600*, ANL-7426 (March 1968).
7. D. A. Kucera and J. T. Madell, "Analysis and Development of Neutron Cross Sections for EBR-II Studies," *Reactor Physics Division Annual Report: July 1, 1967 to June 30, 1968*, ANL-7410, pp. 209-213 (Jan 1969).
8. J. T. Madell, "Investigation of the Temperature Coefficient of EBR-II, Run 25," *Reactor Physics Division Annual Report: July 1, 1966 to June 30, 1967*, ANL-7310, pp. 228-230 (Jan 1968).
9. R. R. Smith and D. L. Mitchell, *Post-irradiation Inspection of Sub-assemblies Discharged from Runs 25 and 26 in EBR-II*, ANL-EBR-002 (March 1969).
10. G. Gajac, J. L. Ratier, M. Reboul, L. Reynes, and M. A. Valantin, "Rapsodie's First Year of Operation," *Proceedings of the International Conference on Sodium Technology and Large Fast Reactor Design: November 7-9, 1968, Part II. Sessions on Large Fast Reactor Design*, ANL-7520, pp. 52-64 (July 1969).
11. J. K. Long, Argonne National Laboratory, private communication (June 1969).

